ACS OMEGA

Open Access

http://pubs.acs.org/journal/acsodf

Article

Synthesis of $BaSiH_6$ Hydridosilicate at High Pressures—A Bridge to $BaSiH_8$ Polyhydride

Doreen C. Beyer, Kristina Spektor,* Olga Yu Vekilova, Jekabs Grins, Paulo H. Barros Brant Carvalho, Logan J. Leinbach, Michael Sannemo-Targama, Shrikant Bhat, Volodymyr Baran, Martin Etter, Asami Sano-Furukawa, Takanori Hattori, Holger Kohlmann, Sergei I. Simak, and Ulrich Häussermann*

Cite This: *ACS Omega* 2025, 10, 15029−15035

Read Online

ACCESS | Metrics & More | Article Recommendations | Supporting Information

ABSTRACT: Hydridosilicates featuring SiH_6 octahedral moieties represent a rather new class of compounds with potential properties relating to hydrogen storage and hydride ion conductivity. Here, we report on the new representative $BaSiH_6$ which was obtained from reacting the Zintl phase hydride $BaSiH_{\sim 1.8}$ with H_2 fluid at pressures above 4 GPa and subsequent decompression to ambient pressure. Its monoclinic crystal structure ($C2/c$, a = 8.5976(3) Å, b = 4.8548(2) Å, c = 8.7330(4) Å, β = 107.92(1)°, Z = 4) was characterized by a combination of synchrotron radiation powder X-ray diffraction, neutron powder diffraction, and DFT calculations. It consists of complex SiH_6^{2-} ions ($d_{Si-H} \approx 1.61$ Å), which are octahedrally coordinated by Ba^{2+} counterions. The arrangement of Ba and Si atoms deviates only slightly from an ideal fcc NaCl structure with $a \approx 7$ Å. IR and Raman spectroscopy showed SiH_6^{2-} bending and stretching modes in the ranges 800−1200 and 1400−1800 cm^{-1}, respectively, in agreement with a hypervalent Si−H bonding situation. $BaSiH_6$ is thermally stable up to 95 °C above which decomposition into BaH_2 and Si takes place. DFT calculations indicated a direct band gap of 2.5 eV and confirmed that at ambient pressure $BaSiH_6$ is a thermodynamically stable compound in the ternary Ba−Si−H system. The discovery of $BaSiH_6$ consolidates the compound class of hydridosilicates, accessible from hydrogenations of silicides at gigapascal pressures (<10 GPa). The structural properties of $BaSiH_6$ suggest that it presents an intermediate (or precursor) for further hydrogenation at considerably higher pressures to the predicted superconducting polyhydride $BaSiH_8$ [Lucrezi, R.; et al. *npj Comput. Mater.* **2022**, *8*, 119] whose structure is also based on a NaCl arrangement of Ba and Si atoms but with Si in a cubic environment of H.

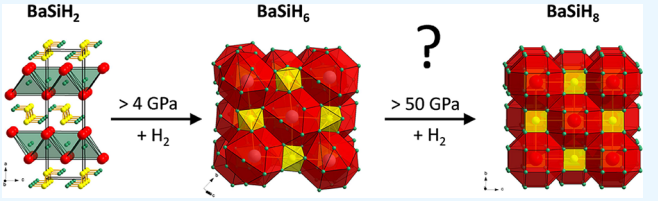

INTRODUCTION

Recently, it has been shown that silicon is capable of forming hydrogen-rich hydridosilicates featuring octahedral SiH_6^{2-} complex ions. Synthesis efforts until today yielded K_2SiH_6, Rb_2SiH_6, and Na_3SiH_7.[1−3] More potential representatives, like Na_2SiH_6, $NaSiH_5$, Li_2SiH_6, have been proposed from computational structure prediction.[3−6] Hydridosilicates are salt-like compounds and their structural chemistry resembles that of well-established fluorosilicates/germanates. However, in contrast with fluorosilicates, hydridosilicates are not insulators but semiconductors. The occurrence of hypervalent SiH_6^{2-} moieties is peculiar since the polarity of the $Si^{\delta+}-H^{\delta-}$ bond is rather small and hypervalence of p-elements is usually associated with electronegative ligands, such as F. It has been suggested that hydridosilicates may have interesting hydride ion conducting and/or hydrogen storage properties,[5] yet the physical, chemical, and materials properties of these compounds remain poorly investigated because of their scarcity.

The synthesis of hydridosilicates typically requires high pressure conditions in the multi GPa range, 4−10 GPa.[1−3] This pressure range is accessible with large-volume press (LVP) high-pressure methodology which provides sizable sample volumes and well-controlled p, T environments for high-pressure hydrogenation reactions.[7−9] In LVP hydrogenations, H_2 has to be delivered by an internal solid source which is integrated in the sample. Ammonia borane, BH_3NH_3, has been recognized as an ideal H-source as it possesses a high H content and decomposes neatly to inert BN and H_2 at comparatively low temperatures (200−400 °C, depending on p).[10] Various types of precursor scenarios may be considered for high pressure hydrogenations potentially leading to hydridosilicates, such as MH_n + Si, M_mSi_n, $M_mSi_nH_x$ (M = active metal), of which the latter, M_mSi_n (silicide Zintl phases) and $M_mSi_nH_x$ (Zintl phase hydrides), have shown largely superior kinetics[2] thus enabling lower synthesis temperatures and potentially access to metastable products.

Received: November 19, 2024
Revised: February 26, 2025
Accepted: March 28, 2025
Published: April 7, 2025

https://doi.org/10.1021/acsomega.4c10502
ACS Omega 2025, 10, 15029−15035

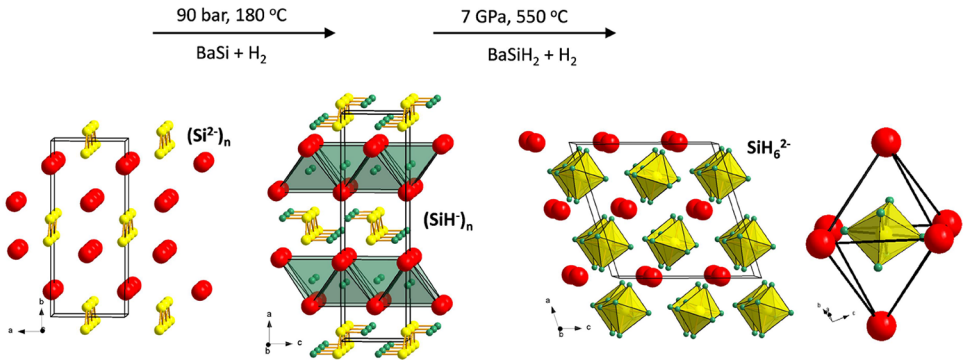

Figure 1. From left to right: low pressure hydrogenation transforms the Zintl phase BaSi (CrB structure type, *Cmcm*, $Z = 4$) into the hydride $BaSiH_{2-x}$ ($x \approx 0.15$; *Pnma*, $Z = 4$),[12] which in turn yields $BaSiH_6$ (*C*2/*c*, $Z = 4$) upon hydrogenation at gigapascal pressures. Ba, Si, and H atoms are depicted as red, yellow, and green circles, respectively. Far right: octahedral coordination of a SiH_6^{2-} ion by six Ba^{2+} counterions in *C*2/*c* $BaSiH_6$ (based on DFT relaxed H atom positions, see text).

We have started to explore more systematically the accessibility and compositional variety of hydridosilicates. Here we report on the synthesis of $BaSiH_6$ from hydrogenation of the Zintl phase hydride $BaSiH_{2-x}$ at ∼7 GPa which resulted in sizable bulk samples with several tens of mg quantities. We find that the structure of $BaSiH_6$ closely relates to that of the even more hydrogen-rich metallic and high T_C superconducting polyhydride $BaSiH_8$ which has been predicted to be thermodynamically stable at ultrahigh pressures, above 100 GPa.[11]

METHODS

Synthesis of $BaSiH_{2-x}$ ($x \approx 0.15$) Precursor. The Zintl phase hydride $BaSiH_{2-x}$ was prepared by sintering BaSi in a hydrogen atmosphere (H_2, Air Liquide, 99.9%) at 90 bar pressure and 180 °C for 24 h using an autoclave made from H-resistant Nicrofer 5219Nb alloy.[12] BaSi in turn was synthesized by arc-melting mixtures of the elements (Si, ChemPur, 99.9999%; Ba rod, 99.3%) with a slight (about 5%) Ba excess. The synthesis of the deuteride $BaSiD_{2-x}$ is described in the Supporting Information section.

Synthesis of $BaSiH_6$. All steps of sample preparation for high pressure (LVP) hydrogenation experiments were performed in an Ar-filled glovebox. NaCl is considered an ideal capsule material since it provides tight seals and resists hydrogen diffusion.[7−9] Powdered precursor $BaSiH_{2-x}$ and hydrogen source BH_3NH_3 (Sigma Aldrich, 97%) were pressed into pellets with an outer diameter (OD) of 4 mm and ∼3 and ∼1.3 mm height, respectively. A precursor pellet was placed between two BH_3NH_3 pellets and sealed in a NaCl capsule (OD 6.1 mm, ∼7.8 mm height). The molar ratio $BaSiH_{2-x}$:BH_3NH_3 corresponded roughly to 1:1 ($BaSiH_{2-x}$:H_2 = 1:3). Two synthesis runs were conducted at Arizona State University (ASU) using the COMPRES 18/12 assemblies.[13] Samples were compressed in a 1000 tonnes press to ∼7 GPa and subsequently heated to 550 °C over two hours, held at this temperature for eight hours, cooled back to room temperature over 1 h, and subsequently decompressed. The temperature was measured with a type C thermocouple. Samples were recovered in a glovebox. In situ diffraction experiments were performed at various pressures between 4 and 19 GPa at the synchrotron facility PETRA III, DESY and at 5 GPa at the neutron facility MLF, J-PARC, employing the LVP beamlines P61B[14] and PLANET,[15] respectively. Results from these experiments will be reported separately. The J-PARC experiment, however, is described in more detail in the SI section.

Powder X-ray Diffraction (PXRD). PXRD patterns of recovered $BaSiH_6$ were collected at the beamline P02.1, PETRA III, DESY[16] using monochromatic synchrotron radiation ($E \approx 60$ keV, $\lambda = 0.20734-0.20738$ Å). Samples produced at P61B were sealed (as sintered pieces without grinding) inside 1.0 mm diameter glass capillaries. For multitemperature measurements, the sample produced at ASU was finely ground and sealed in 0.3 mm diameter fused silica capillaries. Capillaries were heated with a mini hot air blower which is part of the sample environment at P02.1. For indexing of diffraction patterns, the Crysfire package[17] was used. Le Bail analysis and Rietveld refinement of the PXRD data were performed in Jana2006.[18] Further details are provided as SI.

Spectroscopy. FTIR spectra were recorded with a "Golden Gate" micro-ATR accessory using a Varian IR-670 spectrometer with a thermostatted DTGS detector. A powdered sample of $BaSiH_6$ was transferred from the glovebox in an airtight vial. At the spectrometer, the vial was opened, and the powder was quickly clamped between the ATR diamond and sapphire elements. During the transfer process, moisture-sensitive $BaSiH_6$ may have decomposed slightly. For Raman spectroscopy, powdered samples were sealed in 0.3 mm Lindemann capillaries. Spectra were measured using a LabRAM HR 800 spectrometer. The instrument is equipped with an 800 mm focal length spectrograph and a Peltier-cooled (−70 °C), back-thinned CCD detector. Samples were excited using a double-frequency Nd:YAG laser (532 nm). A 10% filter was applied corresponding to a low power density of 5.5×10^{-6} mW·μm^{-2}). Raman spectra were collected with an exposure time of 150 s (100 accumulations) and using a 600 grooves/mm grating.

Theoretical Calculations. Crystal structure prediction (CSP) utilizing the USPEX code[19−21] coupled with the Vienna Ab Initio Simulation Package (VASP)[22,23] was employed for assisting the identification of the monoclinic $BaSiH_6$ structure. For the USPEX calculation, we used the numerical constraints of a fixed composition (1:1:6) and the maximum number of atoms in a candidate cell of 32 ($Z = 4$). The lowest enthalpy structure identified had *C*2/*c* space group symmetry and $Z = 4$. VASP calculations were based on a first-principles projector-augmented wave method[24] within the density functional theory (DFT).[25] The generalized gradient approximation for

https://doi.org/10.1021/acsomega.4c10502
ACS Omega 2025, 10, 15029−15035

exchange and correlation potential and energy was used in its Perdew–Burke–Ernzerhof (PBE) flavor.[26,27] Total energy/electronic structure calculations were performed for BaH_2, $BaSiH_2$, Si, and $BaSiH_6$ on fully relaxed structures. Hydrogen was calculated as a molecule H_2. The Monkhorst–Pack[28] k-point density for integrations over the Brillouin zone was set with 0.2. The energy cutoff for plane waves was 800 eV. Phonon dispersions were calculated with PHONOPY.[29] The required dynamical matrix was obtained via highly accurate calculations with density functional perturbation theory as implemented in VASP, with the energies converged down to 10^{-8} eV.

RESULTS AND DISCUSSION

The Zintl phase BaSi (CrB structure type) features polyanionic zigzag chains of Si atoms ($^1_\infty[Si^{2-}]$).[30] Upon hydrogenation at low-pressure autoclave conditions (90 bar (9 MPa)), the Zintl phase hydride $BaSiH_{2-x}$ is obtained for which the basic structural features of BaSi are retained.[12] In the structure of $BaSiH_{2-x}$, H is located as a hydride (H^-) anion in tetrahedral interstices formed by the Ba atoms. In addition, the zigzag chain Si atoms are decorated with covalently bonded H atoms (thus changing $^1_\infty[Si^{2-}]$ into a $^1_\infty[SiH^-]$ polyanion), Figure 1. However, the site of the H coordinating Si has a slight deficiency of about 15%. Si atoms in $^1_\infty[SiH^-]$ obey the octet rule, and stoichiometric $BaSiH_2$ would correspond to an electronically balanced Zintl phase, i.e., $Ba^{2+}(SiH)^-(H^-)$.[12]

The formation of the hydridosilicate $BaSiH_6$ was initially observed in in situ diffraction experiments when attempting the hydrogenation of $BaSiH_{2-x}$ in the pressure interval 4–13 GPa, and from these experiments, it could also be shown that

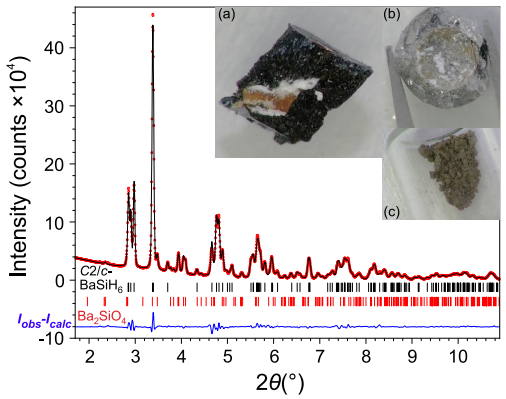

Figure 2. Rietveld fit of the $BaSiH_6$ structure to a synchrotron PXRD pattern (λ = 0.20734 Å). Vertical lines are reflection markers for $BaSiH_6$ and Ba_2SiO_4 impurity. Phase fractions: ∼84(1) wt% (92 mol %) $BaSiH_6$ and ∼16(1) wt% (8 mol%) Ba_2SiO_4. Inset (a) shows a photograph of an orange-colored $BaSiH_6$ sample from an in situ experiment (∼8.5 GPa, 570 °C) before recovery, embedded between BN residual from decomposed BH_3NH_3 inside the NaCl capsule (which attained a black color due to X-ray irradiation). Note that the sample is largely rearranged from its original position during the reaction due to the escape of excess H_2 upon decompression. Inset (b) shows a partially recovered pellet (4 mm diameter) of $BaSiH_6$ from a scaled-up synthesis experiment (the NaCl capsule is partly broken off, and the surface of the pellet is not yet cleaned completely from BN residual), and inset (c) shows a part of this pellet ground into a fine powder inside a vial with a 6 mm diameter. The light brownish/gray color in (b) and (c) is attributed to a small grain size and/or the presence of Si impurity.

Table 1. Results of the Rietveld Refinement of the $BaSiH_6$ Structure at Ambient Conditions

crystal system	monoclinic
space group	$C2/c$ (no. 15)
Z	4
lattice parameters[a]	a = 8.5976(3) Å
	b = 4.8548(2) Å
	c = 8.7330(4) Å
	β = 107.918(4)°
V (Å^3)	346.84(2)
formula weight (g/mol)	171.46
d_{calc} (g/cm^3)	3.284
R_{obs} (%)	1.39
R_{all} (%)	1.39

[a]Pseudocubic triclinic cell: a = 7.040 Å, b = 7.008 Å, c = 7.040 Å, α = 89.32°, β = 87.20°, γ = 89.32°.

$BaSiH_6$ is retained at ambient pressure (Figure 2). Subsequently, dedicated experiments were performed at 7 GPa and 550 °C to scale up its preparation, which for the first time yielded sizable quantities (several tens of mg) of a hydridosilicate. However, although the conversion of $BaSiH_{2-x}$ proceeded quantitatively, all samples (originating from the same batch of $BaSiH_{2-x}$) contained Ba_2SiO_4 (orthosilicate) as an impurity (3–8 mol%) which presumably originates from an oxide/peroxide/hydroxide contamination of the $BaSiH_{2-x}$ precursor (cf. discussion in the SI section). $BaSiH_6$ displays a reddish-orange color as well sintered specimen, but when it is small-grained or as powder, it appears light brownish/gray (insets in Figure 2).

The SR-PXRD pattern of $BaSiH_6$ could be indexed to the monoclinic C-centered cell with Z = 4 that was as suggested from computational CSP (see SI for details). The refinement of the CSP model proceeded highly satisfactorily. Unambiguous confirmation of the H positions came then from an (in situ) neutron diffraction experiment, probing the formation of $BaSiD_6$ at around 5 GPa (see SI for details), which provided a data set at 2.5 GPa and room temperature. To arrive at the H position parameters for $BaSiH_6$ at ambient conditions, it was deemed most consistent to extract them from a DFT relaxation where the lattice parameters and Ba and Si atomic position parameters were constrained to the experimentally refined ones, referring to room temperature and ambient pressure. The resulting structure of $BaSiH_6$ after the refinement is reported in Tables 1 and 2 (see also Figure 2 and SI section). It resembles closely the unique KPF_6-III structure, which apparently was determined over 30 years ago[31] but has come to attention only recently.[32]

The monoclinic crystal structure of $BaSiH_6$ is built of Ba^{2+} and octahedral complex ions SiH_6^{2-} which are the characteristic constituents of hydridosilicates. The SiH_6^{2-} octahedra appear in two orientations, which are related through 2_1 symmetry axes. They are hosted within irregular octahedra of Ba^{2+} counterions (d_{Ba-Ba} = 4.78–5.26 Å) with their corners pointing to triangle faces and edges of the Ba_6 octahedron (Figure 1). The monoclinic unit cell blurs an almost ideal NaCl-type arrangement of cations and centers of complex anions (Figure 3), which is realized in the fcc structure of $NaPF_6$ (with PF_6^- octahedra aligned in the same orientation as the Na_6 ones)[33] but from which monoclinic KPF_6 severely deviates. The parameters of the pseudocubic triclinic unit cell of $BaSiH_6$ are in the range 7.01–7.04 Å and 87.2–89.3° (Table

https://doi.org/10.1021/acsomega.4c10502
ACS Omega 2025, 10, 15029–15035

Table 2. Fractional Coordinates and Atomic Displacement Parameters (ADPs) for the $BaSiH_6$ Structure at Ambient Conditions[a]

atom	Wyck	*x*	*y*	*z*	U_{iso} (Å^2)	B_{iso} (Å^2)
Ba	4*e*	0	0.6990(2)[b]	0	0.0198(3)	1.56(2)
Si	4*d*	1/4	1/4	1/2	0.0181(9)	1.43(7)
H1	8*f*	0.8091	0.4674	0.4394	0.038	3
H2	8*f*	0.4384	0.3133	0.5963	0.038	3
H3	8*f*	0.2327	0.0912	0.6531	0.038	3

[a]Hydrogen atom positions were obtained from DFT relaxation constraint to the experimental lattice, see text. The coordinates and ADPs of the H atoms remained fixed during the refinement. [b]Ba is at 4*e* (0, 0.75, 0) for an idealized NaCl-type arrangement of Ba and Si atoms.

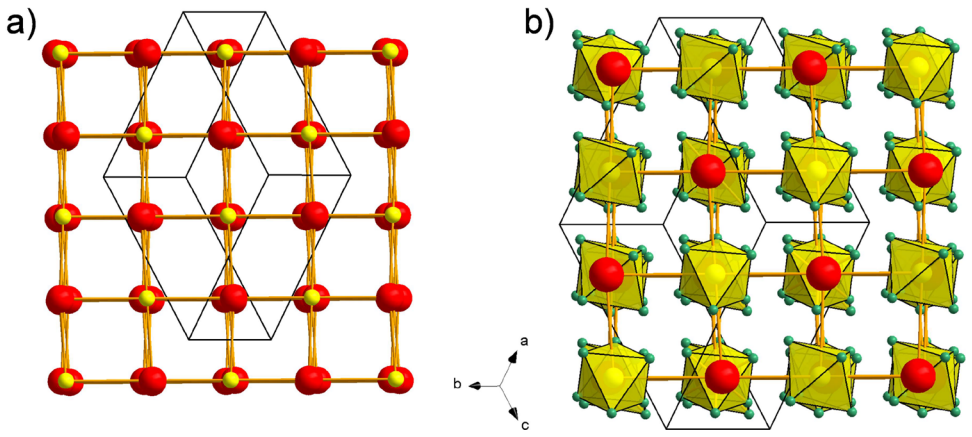

Figure 3. (a) Projection of the monoclinic $BaSiH_6$ structure showing a nearly ideal fcc NaCl structure arrangement of Ba and Si atoms (red and yellow spheres, respectively). In (b) the H atoms are added (green spheres).

Table 3. Relevant Interatomic Distances in $BaSiH_6$[a]

atom pair			*d* (Å)	atom pair			*d* (Å)
Si	H2	×2	1.590	Ba	Ba	×2	4.775
	H3	×2	1.608		Ba	×2	4.855
	H1	×2	1.609		Ba	×4	4.937
Ba	Si	×2	3.354		Ba	×2	5.123
	Si	×2	3.512		Ba	×2	5.254
	Si	×2	3.695	Ba	H3	×2	2.605
Si	Si	×2	4.855		H3	×2	2.607
	Si	×4	4.937		H2	×2	2.693
	Si	×4	4.996		H2	×2	2.798
	Si	×2	5.099		H1	×2	2.822
					H1	×2	2.892
					H1	×2	2.965
					H2	×2	3.274

[a]Estimated standard deviations are either smaller than 0.001 Å or not defined (when involving H atoms).

3). Nearest neighbor Ba−Si distances are between 3.35 and 3.70 Å.

The local point group symmetry of the SiH_6^{2-} ion is C_i, and there are two octahedra in the primitive unit cell. Despite the low symmetry, the Si−H distances are almost equal (d_{Si-H} = 1.60−1.62 Å) and angles are close to ideal (89−91°). Consequently, one would expect that the internal modes of SiH_6^{2-} follow the O_h pattern of three stretching modes (A_{1g}, E_g, T_{1u}) and three bending modes (T_{2g}, T_{1u}, T_{2u}) and that the O_h selection rules are largely obeyed.[32,34] The IR and Raman spectra of $BaSiH_6$, shown in Figure 4, reveal the location of bending and stretching modes between 800−1250 and 1400−1810 cm^{-1}, respectively, which is also seen in the DFT calculated zone center optical modes. The Raman spectrum

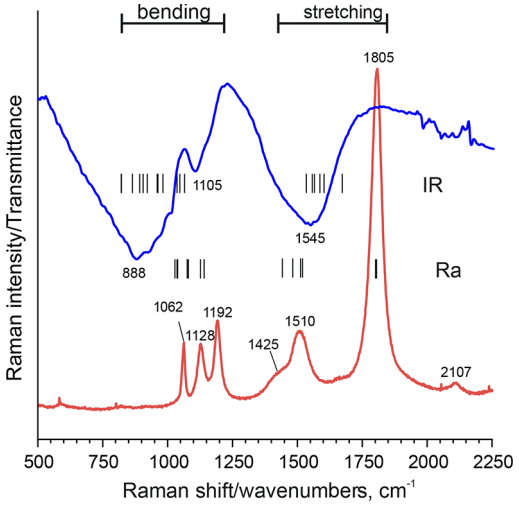

Figure 4. Raman (lower curve) and IR spectrum (upper curve) of $BaSiH_6$. The bars represent the position of DFT calculated Si−H stretching and bending modes. The unassigned band at 2107 cm^{-1} in the Raman spectrum may correspond to an overtone. Note that Si−O bands from Ba_2SiO_4 orthosilicate impurity are expected to be below 1000 cm^{-1} and will not interfere with $BaSiH_6$ Si−H bands in the Raman spectrum.[36] In contrast, in the IR spectrum, Si−O stretching and Si−O−H bending bands from partial decomposition of the sample may be present.

shows six vibrational bands, three in the stretching and three in the bending mode regions, which implies that the O_h-degenerate modes E_g (stretch) and T_{1g} (bend) all appear considerably split by several tens of cm^{-1}. The removal of the O_h degeneracy is not visible in the IR spectrum, which only shows two broad bands, one in the stretching region

https://doi.org/10.1021/acsomega.4c10502
ACS Omega 2025, 10, 15029−15035

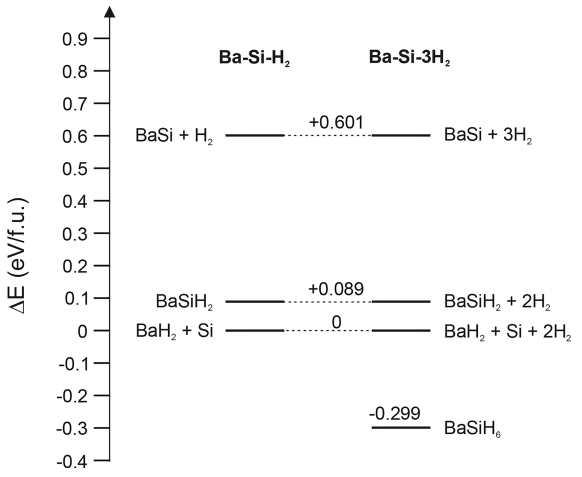

Figure 5. DFT calculated energy differences for the pseudobinary compositions $BaSi-H_2$ and $BaSi-3H_2$.

(accounting for T_{1u}) and one in the bending region (accounting for T_{1u} and the O_h-forbidden T_{2u}). An additional IR signal may come from Fermi resonance,[33] but this is not clear. The symmetric stretch is at the highest wavenumber, around 1800 cm^{-1}, which relates well to K_2SiH_6 and Rb_2SiH_6 (which are also built of separated SiH_6^{2-} octahedra but with local point group symmetry O_h).[1] The associated Si−H stretching force constant is thus considered similar (~1.3 N/cm),[35] confirming that SiH_6^{2-} is a weakly bonded moiety compared to regular-valent silicon hydride species.[2]

The electronic band structure of $BaSiH_6$ shows considerable dispersion of the occupied bands (1−3 eV), as depicted in Figure S7. Yet these bands reflect clearly the molecular orbital energy levels of octahedral SiH_6^{2-} (i.e., a_{1g}, t_{1u}, e_g) which confirms the ionic character of this compound. The highest lying e_g-type band is nonbonding and primarily composed of H states. The band gap appears to be direct with a size of about 2.5 eV. Typically, DFT calculated band gaps are underestimated when using the PBE functional. Here, however, the reddish appearance of a sintered bulk sample (cf. Figure 2, inset) suggests quite good agreement.

Multitemperature PXRD measurements revealed a limited thermal stability of $BaSiH_6$. At about 95 °C, decomposition onset to BaH_2 and Si is observed (Figure S4). Nevertheless, according to DFT calculations, $BaSiH_6$ is a thermodynamically stable compound (with respect to the most stable component mixture BaH_2 + Si + H_2). In fact, at ambient pressure, $BaSiH_6$ represents the only stable ternary compound in the Ba−Si−H system, whereas the (stoichiometric) Zintl phase hydride $BaSiH_2$ is not (Figure 5). This follows earlier observations that hydridosilicates appear generally thermodynamically stable at ambient pressure, albeit high pressure is needed for their synthesis for raising thermal stability beyond required reaction temperatures. In this respect, and as mentioned earlier, silicide Zintl phases (or also Zintl phase hydrides) can favorably act as reactive precursors with low kinetic barriers for hydrogenation.

Recently, Lucrezi et al. reported a computational study of the even more hydrogen-rich polyhydride $BaSiH_8$.[11] $BaSiH_8$ was predicted to be thermodynamically stable at pressures above 130 GPa. However, minimum pressures for dynamic and kinetic stability (which are the important parameters for retaining a high-pressure material toward ambient pressure) were found to be considerably lower, at around 25 and 30 GPa, respectively.[11,37] $BaSiH_8$ is potentially a promising superconducting material with a critical temperature T_C around 80 K (rather independent of pressure). The existence of $BaSiH_6$ was not known to these authors and also their results were based on zero Kelvin calculations. In light of our findings, it would be interesting and also important to reassess thermodynamic, kinetic, and dynamic stabilities for $BaSiH_8$, considering both the presence of $BaSiH_6$ in the ternary system Ba−Si−H and elevated temperatures of >400 °C necessary for inducing reactions.

Here, we infer that $BaSiH_6$ represents a precursor, or intermediate, to the higher hydride $BaSiH_8$, potentially accessible at pressures by far exceeding 10 GPa, and motivate this by their close structural relationship. In cubic $BaSiH_8$ (space group $Fm\bar{3}m$), Ba and Si atoms form an ideal NaCl-type structure arrangement. H atoms are situated on the 32*f* (*x*,*x*,*x*) position) and surround the Si atoms cubically. Interestingly, the calculated lattice parameter of $BaSiH_8$ at ambient pressure (where $BaSiH_8$ would be both dynamically and kinetically unstable) is close to 7 Å,[11,37] implying an almost equal dimension of the NaCl lattice hosting SiH_6 octahedra in $BaSiH_6$ and SiH_8 cubes in $BaSiH_8$ (Figure 6). Obviously, the "insertion" of additional 2 H atoms per formula unit into the $BaSiH_6$ structure will change the Ba−H coordination

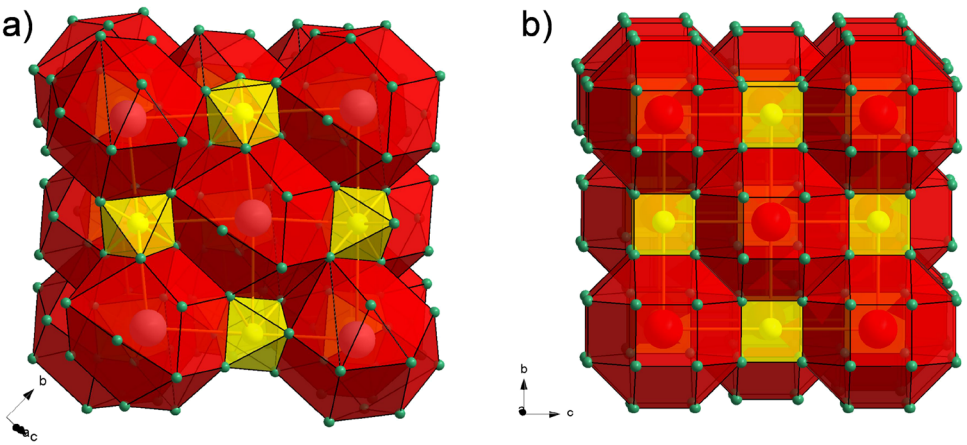

Figure 6. Comparison of the crystal structures of monoclinic $BaSiH_6$ (a) and cubic $BaSiH_8$ (b). Ba and Si coordination by H are depicted as red and yellow polyhedra, respectively.

https://doi.org/10.1021/acsomega.4c10502
ACS Omega 2025, 10, 15029−15035

drastically. In $BaSiH_8$, Ba is coordinated by 24 H atoms, forming a rhombicuboctahedron at a distance 2.87 Å, whereas in $BaSiH_6$, Ba is coordinated rather irregularly by 14 H atoms in a distance range 2.61−2.97 Å.

CONCLUSIONS

The hydridosilicate $BaSiH_6$ can be synthesized when reacting the Zintl phase hydride $BaSiH_{2-x}$ with H_2 fluid at pressures above 4 GPa and subsequent decompression to ambient pressure. The monoclinic crystal structure consists of Ba^{2+} and hypervalent complex SiH_6^{2-} ions. Their mutual arrangement corresponds closely to an ideal fcc NaCl structure. $BaSiH_6$ is the first hydridosilicate with an alkaline earth metal and its discovery suggests a broader compositional variability in the cationic constituents of this relatively new class of compounds. Like the previously described alkali metal hydridosilicates, $BaSiH_6$ is a thermodynamically stable compound at ambient pressure, albeit with a rather low thermal stability. Its synthesis via $BaSiH_{2-x}$ can be upscaled which eventually, with pure samples, will allow for detailed physical property characterization/measurements, including heat capacity, dynamic properties from inelastic/quasielastic neutron scattering spectroscopy, semiconductor properties, and H^- ion conductivity (probably only seen at pressure upon increased thermal stability). The structural properties of $BaSiH_6$ suggest that it represents a bridge to the predicted superconducting polyhydride $BaSiH_8$[11] which can be expected from hydrogenations at ultrahigh pressures of about 100 GPa and for which $BaSiH_6$ may serve as a most suitable precursor.

ASSOCIATED CONTENT

Supporting Information

The Supporting Information is available free of charge at https://pubs.acs.org/doi/10.1021/acsomega.4c10502.

> Detailed description of synthesis and sample preparations; details of the PXRD characterization of products; detailed description of the high-pressure neutron diffraction experiment and the refinement of neutron diffraction data; structure parameters for $BaSiD_6$ at 2.5 GPa; detailed description of the multitemperature synchrotron powder diffraction experiment and evaluation of data; DFT relaxed structure parameters of for $C2/c$ $BaSiH_6$; and electronic band structure and density of states for $C2/c$ $BaSiH_6$ (PDF)

Accession Codes

Deposition Numbers 2420757 and 2420758 contain the supplementary crystallographic data for this paper. These data can be obtained free of charge via the joint Cambridge Crystallographic Data Centre (CCDC) and Fachinformationszentrum Karlsruhe Access Structures service.

AUTHOR INFORMATION

Corresponding Authors

Kristina Spektor − *Deutsches Elektronen-Synchrotron DESY, D-22607 Hamburg, Germany;* orcid.org/0000-0002-3267-9797; Email: Kristina.Spektor@gmail.com

Ulrich Häussermann − *Department of Materials and Environmental Chemistry, Stockholm University, SE-10691 Stockholm, Sweden;* orcid.org/0000-0003-2001-4410; Email: Ulrich.Haussermann@mmk.su.se

Authors

Doreen C. Beyer − *Institute for Inorganic Chemistry and Crystallography, Leipzig University, D-04103 Leipzig, Germany*

Olga Yu Vekilova − *Department of Materials and Environmental Chemistry, Stockholm University, SE-10691 Stockholm, Sweden*

Jekabs Grins − *Department of Materials and Environmental Chemistry, Stockholm University, SE-10691 Stockholm, Sweden*

Paulo H. Barros Brant Carvalho − *Department of Chemistry−Ångström, Uppsala University, SE-75121 Uppsala, Sweden*

Logan J. Leinbach − *Eyring Materials Center, Arizona State University, Tempe, Arizona 85287, United States*

Michael Sannemo-Targama − *Department of Materials and Environmental Chemistry, Stockholm University, SE-10691 Stockholm, Sweden*

Shrikant Bhat − *Deutsches Elektronen-Synchrotron DESY, D-22607 Hamburg, Germany;* orcid.org/0000-0002-1229-9842

Volodymyr Baran − *Deutsches Elektronen-Synchrotron DESY, D-22607 Hamburg, Germany;* orcid.org/0000-0003-2379-3632

Martin Etter − *Deutsches Elektronen-Synchrotron DESY, D-22607 Hamburg, Germany*

Asami Sano-Furukawa − *J-PARC Center, Japan Atomic Energy Agency, Naka-gun, Ibaraki 319-1195, Japan*

Takanori Hattori − *J-PARC Center, Japan Atomic Energy Agency, Naka-gun, Ibaraki 319-1195, Japan*

Holger Kohlmann − *Institute for Inorganic Chemistry and Crystallography, Leipzig University, D-04103 Leipzig, Germany;* orcid.org/0000-0002-8873-525X

Sergei I. Simak − *Theoretical Physics Division, Department of Physics, Chemistry and Biology (IFM), Linköping University, SE-581 83 Linköping, Sweden; Department of Physics and Astronomy, Uppsala University, SE-75120 Uppsala, Sweden*

Complete contact information is available at: https://pubs.acs.org/10.1021/acsomega.4c10502

Notes

The authors declare no competing financial interest.

ACKNOWLEDGMENTS

This research has been supported by the Swedish Research Council (VR) through project 2019-06063 and the Bundesministerium fuer Bildung und Forschung (BMBF)—German Federal Ministry of Education and Research (grant No. 05K20OLA awarded to HK). We are grateful to Per Mistenius for skillfully manufacturing the miniature press dies used for sample preparation. The computations were enabled by resources provided by the National Academic Infrastructure for Supercomputing in Sweden (NAISS), partially funded by the Swedish Research Council through grant agreement no. 2022-06725. S.I.S. acknowledges the support from the Swedish Research Council (VR) (2023-05247) and the ERC (synergy grant FASTCORR project 854843). We acknowledge DESY (Hamburg, Germany), a member of the Helmholtz Association HGF, for the provision of experimental facilities. Parts of this research were carried out at the Facility for Open Research in a Compressed Environment (FORCE) at ASU which is supported by the National Science Foundation under Mid-

Scale Research Infrastructure-1 grant 2131833, and the PETRA III beamlines P61B and P02.1. Beamtime at P02.1 was allocated by an In-House contingent. Beamtimes at P61B were allocated for proposal I-20210167 EC. We are grateful to Dr. Robert Farla for his support during P61B experiments.

REFERENCES

(1) Puhakainen, K.; Benson, D.; Nylén, J.; Konar, S.; Stoyanov, E.; Leinenweber, K.; Häussermann, U. Hypervalent Octahedral SiH_6^{2-} Species from High-Pressure Synthesis. *Angew. Chem., Int. Ed.* **2012**, *51* (13), 3156−3160.
(2) Vekilova, O. Yu.; Beyer, D. C.; Bhat, S.; Farla, R.; Baran, V.; Simak, S. I.; Kohlmann, H.; Häussermann, U.; Spektor, K. Formation and Polymorphism of Semiconducting K_2SiH_6 and Strategy for Metallization. *Inorg. Chem.* **2023**, *62* (21), 8093−8100.
(3) Spektor, K.; Kohlmann, H.; Druzhbin, D.; Crichton, W. A.; Bhat, S.; Simak, S. I.; Vekilova, O. Y.; Häussermann, U. Hypervalent Hydridosilicate in the Na−Si−H System. *Front. Chem.* **2023**, *11*, No. 1251774.
(4) Liang, T.; Zhang, Z.; Feng, X.; Jia, H.; Pickard, C. J.; Redfern, S. A. T.; Duan, D. Ternary Hypervalent Silicon Hydrides via Lithium at High Pressure. *Phys. Rev. Mater.* **2020**, *4* (11), No. 113607.
(5) Liang, T.; Zhang, Z.; Yu, H.; Cui, T.; Feng, X.; Pickard, C. J.; Duan, D.; Redfern, S. A. T. Pressure-Induced Superionicity of H^- in Hypervalent Sodium Silicon Hydrides. *J. Phys. Chem. Lett.* **2021**, *12* (30), 7166−7172.
(6) Wu, S.; Li, B.; Chen, Z.; Hou, Y.; Bai, Y.; Hao, X.; Yang, Y.; Liu, S.; Cheng, J.; Shi, Z. Phase Transitions and Superconductivity in Ternary Hydride Li_2SiH_6 at High Pressures. *J. Appl. Phys.* **2022**, *131* (6), No. 065901.
(7) Saitoh, H.; Machida, A.; Aoki, K. Synchrotron X-Ray Diffraction Techniques for in Situ Measurement of Hydride Formation under Several Gigapascals of Hydrogen Pressure. *Chin. Sci. Bull.* **2014**, *59* (36), 5290−5301.
(8) Spektor, K.; Crichton, W. A.; Filippov, S.; Klarbring, J.; Simak, S. I.; Fischer, A.; Häussermann, U. Na−Ni−H Phase Formation at High Pressures and High Temperatures: Hydrido Complexes $[NiH_5]^{3-}$ *Versus* the Perovskite $NaNiH_3$. *ACS Omega* **2020**, *5* (15), 8730−8743.
(9) Spektor, K.; Crichton, W. A.; Filippov, S.; Simak, S. I.; Fischer, A.; Häussermann, U. Na_3FeH_7 and Na_3CoH_6: Hydrogen-Rich First-Row Transition Metal Hydrides from High Pressure Synthesis. *Inorg. Chem.* **2020**, *59* (22), 16467−16473.
(10) Nylén, J.; Sato, T.; Soignard, E.; Yarger, J. L.; Stoyanov, E.; Häussermann, U. Thermal Decomposition of Ammonia Borane at High Pressures. *J. Chem. Phys.* **2009**, *131* (10), 104506.
(11) Lucrezi, R.; Di Cataldo, S.; von der Linden, W.; Boeri, L.; Heil, C. In-Silico Synthesis of Lowest-Pressure High-T_c Ternary Superhydrides. *npj Comput. Mater.* **2022**, *8*, 119.
(12) Auer, H.; Guehne, R.; Bertmer, M.; Weber, S.; Wenderoth, P.; Hansen, T. C.; Haase, J.; Kohlmann, H. Hydrides of Alkaline Earth−Tetrel (AeTt) Zintl Phases: Covalent Tt−H Bonds from Silicon to Tin. *Inorg. Chem.* **2017**, *56* (3), 1061−1071.
(13) Stoyanov, E.; Häussermann, U.; Leinenweber, K. Large-Volume Multianvil Cells Designed for Chemical Synthesis at High Pressures. *High Pressure Res.* **2010**, *30* (1), 175−189.
(14) Farla, R.; Bhat, S.; Sonntag, S.; Chanyshev, A.; Ma, S.; Ishii, T.; Liu, Z.; Néri, A.; Nishiyama, N.; Faria, G. A.; Wroblewski, T.; Schulte-Schrepping, H.; Drube, W.; Seeck, O.; Katsura, T. Extreme Conditions Research Using the Large-Volume Press at the P61B Endstation, PETRA III. *J. Synchrotron Rad.* **2022**, *29* (2), 409−423.
(15) Hattori, T.; Sano-Furukawa, A.; Arima, H.; Komatsu, K.; Yamada, A.; Inamura, Y.; Nakatani, T.; Seto, Y.; Nagai, T.; Utsumi, W.; Iitaka, T.; Kagi, H.; Katayama, Y.; Inoue, T.; Otomo, T.; Suzuya, K.; Kamiyama, T.; Arai, M.; Yagi, T. Design and Performance of High-Pressure PLANET Beamline at Pulsed Neutron Source at J-PARC. *Nucl. Instrum. Methods Phys. Res., Sect. A* **2015**, *780*, 55−67.
(16) Dippel, A.-C.; Liermann, H.-P.; Delitz, J. T.; Walter, P.; Schulte-Schrepping, H.; Seeck, O. H.; Franz, H. Beamline P02.1 at PETRA III for High-Resolution and High-Energy Powder Diffraction. *J. Synchrotron Rad.* **2015**, *22* (3), 675−687.
(17) Shirley, R. *Crysfire 2004: An interactive powder indexing support system*; Crysfire: Surrey, UK, 2004.
(18) Petříček, V.; Dušek, M.; Palatinus, L. Crystallographic Computing System JANA2006: General Features. *Z. Kristallogr. - Cryst. Mater.* **2014**, *229* (5), 345−352.
(19) Oganov, A. R.; Glass, C. W. Crystal Structure Prediction Using Ab Initio Evolutionary Techniques: Principles and Applications. *J. Chem. Phys.* **2006**, *124* (24), 244704.
(20) Lyakhov, A. O.; Oganov, A. R.; Stokes, H. T.; Zhu, Q. New Developments in Evolutionary Structure Prediction Algorithm USPEX. *Comput. Phys. Commun.* **2013**, *184* (4), 1172−1182.
(21) Oganov, A. R.; Lyakhov, A. O.; Valle, M. How Evolutionary Crystal Structure Prediction Works—and Why. *Acc. Chem. Res.* **2011**, *44* (3), 227−237.
(22) Kresse, G.; Hafner, J. Ab Initio Molecular Dynamics for Liquid Metals. *Phys. Rev. B* **1993**, *47* (1), 558−561.
(23) Kresse, G.; Furthmüller, J. Efficient Iterative Schemes for Ab Initio Total-Energy Calculations Using a Plane-Wave Basis Set. *Phys. Rev. B* **1996**, *54* (16), 11169.
(24) Blöchl, P. E. Projector Augmented-Wave Method. *Phys. Rev. B* **1994**, *50* (24), 17953−17979.
(25) Hohenberg, P.; Kohn, W. Inhomogeneous Electron Gas. *Phys. Rev.* **1964**, *136* (3B), B864−B871.
(26) Perdew, J. P.; Burke, K.; Ernzerhof, M. Generalized Gradient Approximation Made Simple. *Phys. Rev. Lett.* **1996**, *77* (18), 3865−3868.
(27) Perdew, J. P.; Burke, K.; Ernzerhof, M. Errata: Generalized Gradient Approximation Made Simple [Phys. Rev. Lett. 77, 3865 (1996)]. *Phys. Rev. Lett.* **1997**, *78* (7), 1396.
(28) Monkhorst, H. J.; Pack, J. D. Special Points for Brillouin-Zone Integrations. *Phys. Rev. B* **1976**, *13* (12), 5188−5192.
(29) Togo, A.; Tanaka, I. First Principles Phonon Calculations in Materials Science. *Scr. Mater.* **2015**, *108*, 1−5.
(30) Currao, A.; Curda, J.; Nesper, R. Kann man die Arten von Zintl-Anionen steuern?? Variationen über das Thema Si^{2-} im System Sr/Mg/Si. *Z. Anorg. Allg. Chem.* **1996**, *622* (1), 85−94.
(31) Cockcroft, J. K. Neutron-Scattering Studies of Order-Disorder Transitions in Hexafluoride Salts ABF_6. Thesis (D.Phil.), University of Oxford, 1985.
(32) Parker, S. F.; Williams, K. P. J.; Smith, T.; Ramirez-Cuesta, A. J.; Daemen, L. L. Vibrational Spectroscopy of Hexahalo Complexes. *Inorg. Chem.* **2022**, *61* (15), 5844−5854.
(33) Kitashita, K.; Hagiwara, R.; Ito, Y.; Tamada, O. Crystal Structures of Some Cubic Hexafluorophosphates at Ambient Temperatures. *J. Fluorine Chem.* **2000**, *101* (2), 173−179.
(34) Parker, S. F. Spectroscopy and Bonding in Ternary Metal Hydride Complexes—Potential Hydrogen Storage Media. *Coord. Chem. Rev.* **2010**, *254* (3−4), 215−234.
(35) Kranak, V. F.; Lin, Y.-C.; Karlsson, M.; Mink, J.; Norberg, S. T.; Häussermann, U. Structural and Vibrational Properties of Silyl (SiH_3^-) Anions in $KSiH_3$ and $RbSiH_3$: New Insight into Si−H Interactions. *Inorg. Chem.* **2015**, *54* (5), 2300−2309.
(36) Handke, M.; Urban, M. IR and Raman Spectra of Alkaline Earth Metals Orthosilicates. *J. Mol. Struct.* **1982**, *79*, 353−356.
(37) Lucrezi, R.; Kogler, E.; Di Cataldo, S.; Aichhorn, M.; Boeri, L.; Heil, C. Quantum Lattice Dynamics and Their Importance in Ternary Superhydride Clathrates. *Comm* **2023**, *6*, 298.

https://doi.org/10.1021/acsomega.4c10502
ACS Omega 2025, 10, 15029−15035